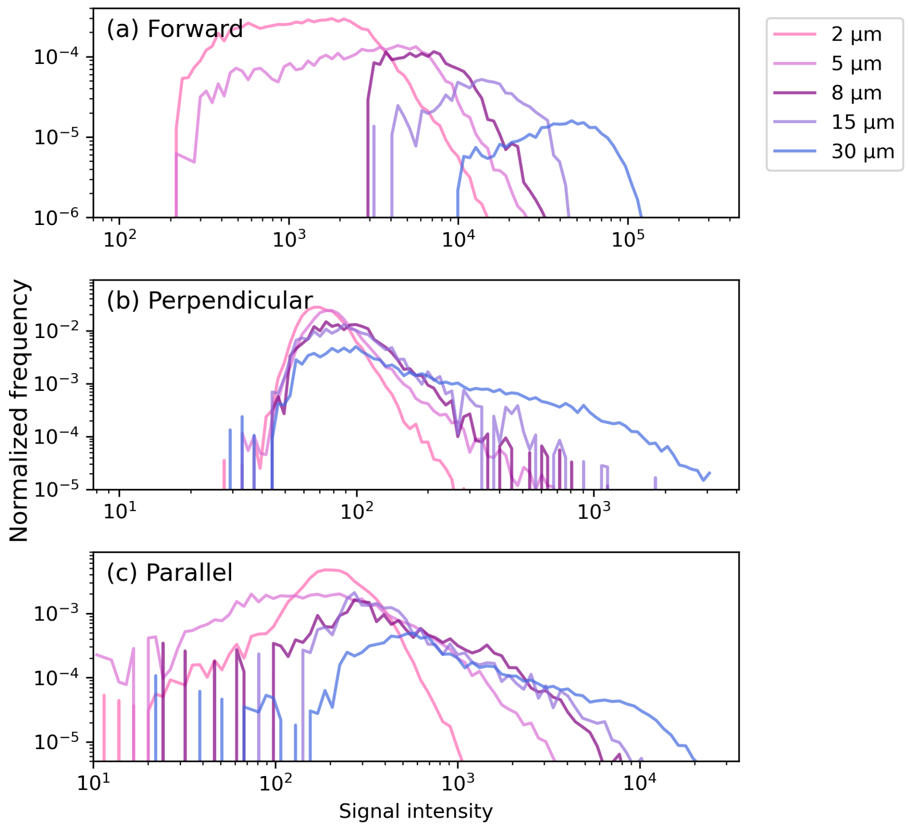

Figure S1. Signal intensity distributions of the different calibration glass beads for all three detectors of the GFAS. (a) Forward scattering signal intensity show a distinct change in distibution with increasing diameter, (b) and (c) are the perpendicular and parallel backward scattering signal intensities, respectively. It is visible in (b) and (c) that the calibration with glass beads is not useful for the backward scattering detectors because the distributions overlap too much to find a reasonable size dependence. Note that in (a), glass bead distribution 8-30 μm have been cut at the lower end due to a high noise peak.

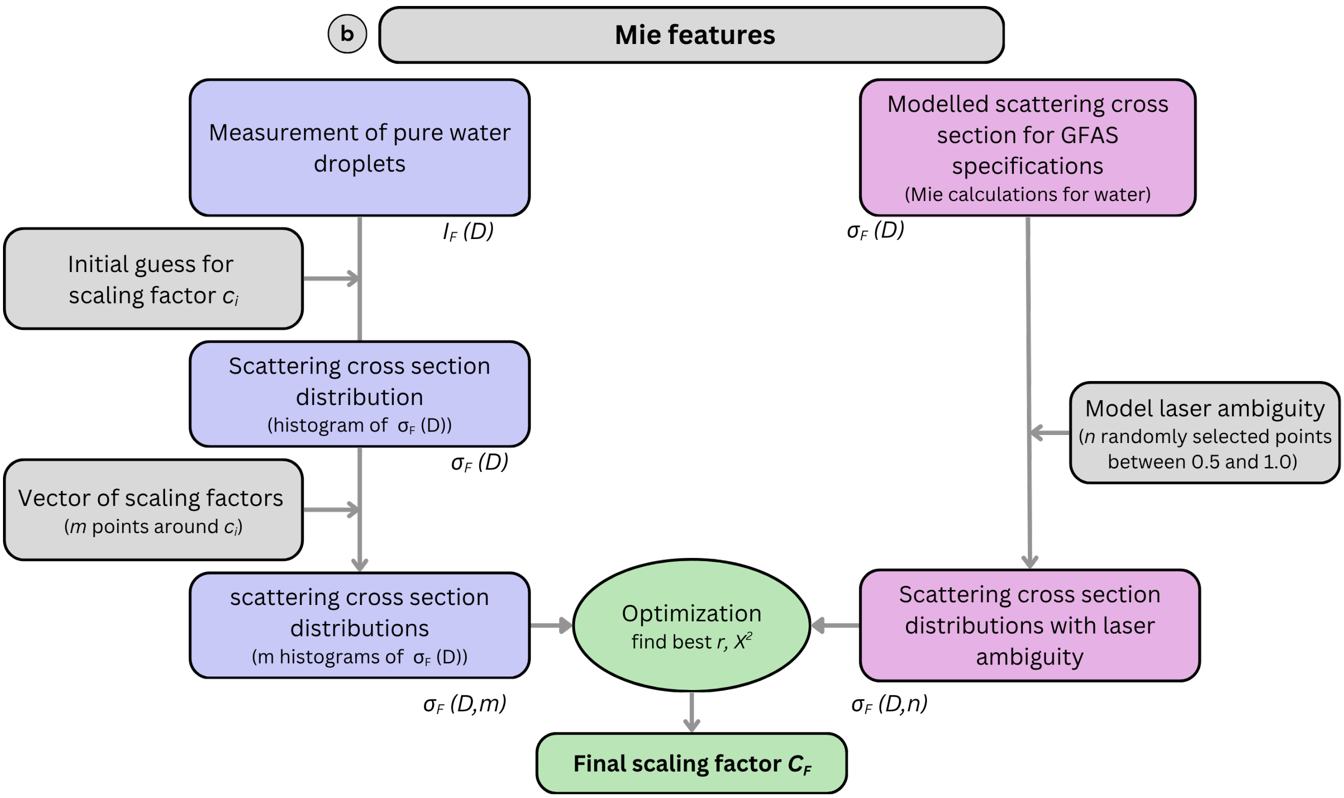

Figure S2. Process of deriving the scale factor c_F by using Mie features in the size distribution. Violet boxes describe the processing steps for measured water droplets, purple boxes describe the processing steps of the modelled measurement response, grey boxes describe inputs for the processing, and describe green boxes the statistics to derive the final scale factor. I_F: scattering intensity measured by the GFAS, σ_F: scattering cross section (cm^2) modeled, D: particle diameter.

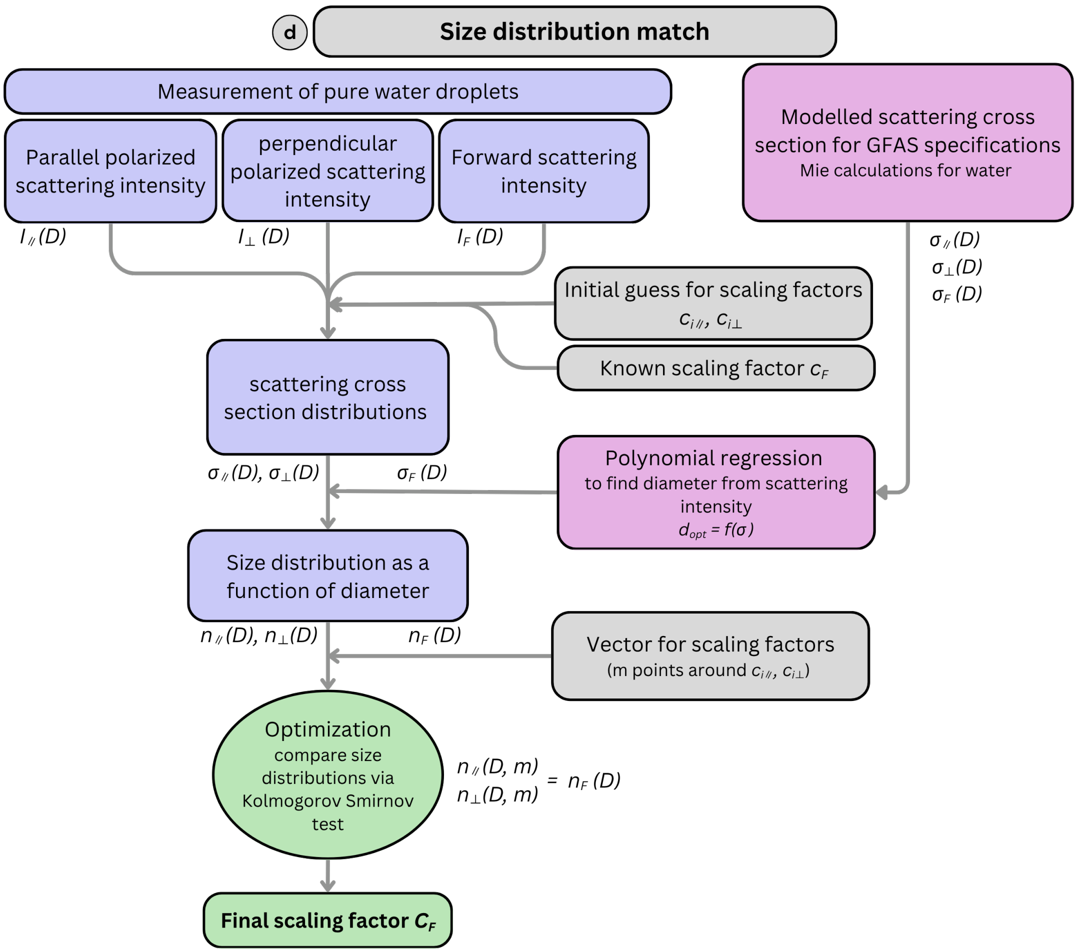

Figure S3. Process of deriving the scale factors $c_{\perp}$ and $c_{||}$ by matching size distributions. Violet boxes describe the processing steps for measured water droplets, purple boxes describe the processing steps of the modelled measurement response, grey boxes describe inputs for the processing, and describe green boxes the statistics to derive the final scale factor. I_F: scattering intensity measured by the GFAS, σ_F: scattering cross section (cm^2) modeled, D: particle diameter.

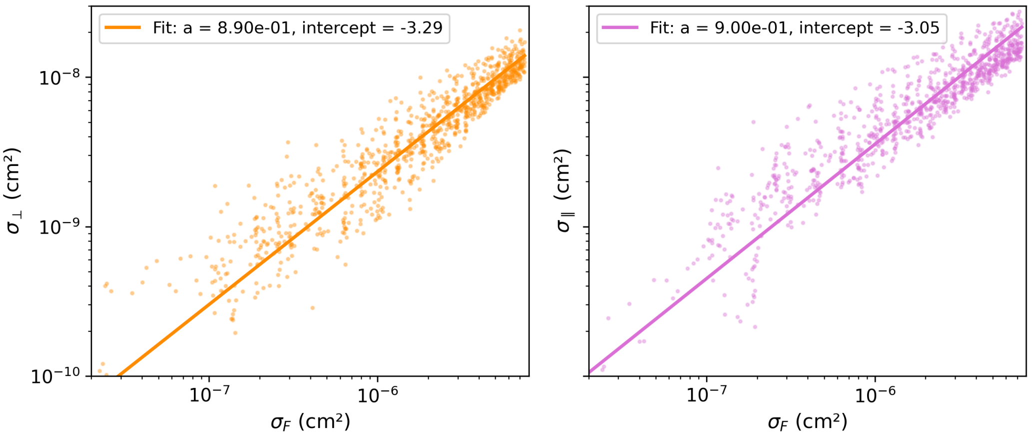

Figure S4. Linear relationship in log-log space between the forward and polarized backward scattering cross sections. Scattering cross sections σ of the forward scattering (F), perpendicular ($\perp$), and parallel ($\|$) polarized backward scattering and their linear relationship in log-log space (Fit): $\log_{10}(\sigma_i) = a \cdot \log_{10}(\sigma_F) + b$ with $i = \|$ or $\perp$.

Table S1. Size threshold table for the GFAS unit of this work. Size bins were chosen in order to minimize sizing errors due to Mie-oscillations. The first row corresponds to the lower bin cutoff of the 27 bins. The GFAS signal intensity for each bin limit was calculated via auto-calibration and the linear fit described within this chapter.

d_{opt} (μm)	σ_F(cm^2)	GFAS signal intensity
0.85	$6.467514 \cdot 10^{-09}$	155.2
3.00	$8.379003 \cdot 10^{-08}$	2011.0
4.90	$1.529953 \cdot 10^{-07}$	3671.9
6.20	$2.012658 \cdot 10^{-07}$	4830.4
7.00	$2.362803 \cdot 10^{-07}$	5670.7
8.50	$3.017956 \cdot 10^{-07}$	7243.1
9.50	$3.182005 \cdot 10^{-07}$	7636.8
12.00	$5.436148 \cdot 10^{-07}$	13046.8
14.00	$7.488419 \cdot 10^{-07}$	17972.2
16.00	$9.142124 \cdot 10^{-07}$	21941.1
18.00	$1.106629 \cdot 10^{-06}$	26559.1
21.00	$1.473284 \cdot 10^{-06}$	35358.8
22.50	$1.574132 \cdot 10^{-06}$	37779.2
24.60	$1.880745 \cdot 10^{-06}$	45137.9
26.50	$2.217868 \cdot 10^{-06}$	53228.8
28.00	$2.499012 \cdot 10^{-06}$	59976.3
31.00	$2.979361 \cdot 10^{-06}$	71504.7
33.50	$3.332257 \cdot 10^{-06}$	79974.2
36.00	$3.977179 \cdot 10^{-06}$	95452.3
37.50	$4.312706 \cdot 10^{-06}$	103504.9
40.00	$4.713859 \cdot 10^{-06}$	113132.6
42.00	$5.278760 \cdot 10^{-06}$	126690.2
44.00	$5.694798 \cdot 10^{-06}$	136675.1
48.00	$6.903932 \cdot 10^{-06}$	165694.4
50.00	$7.420992 \cdot 10^{-06}$	178103.8

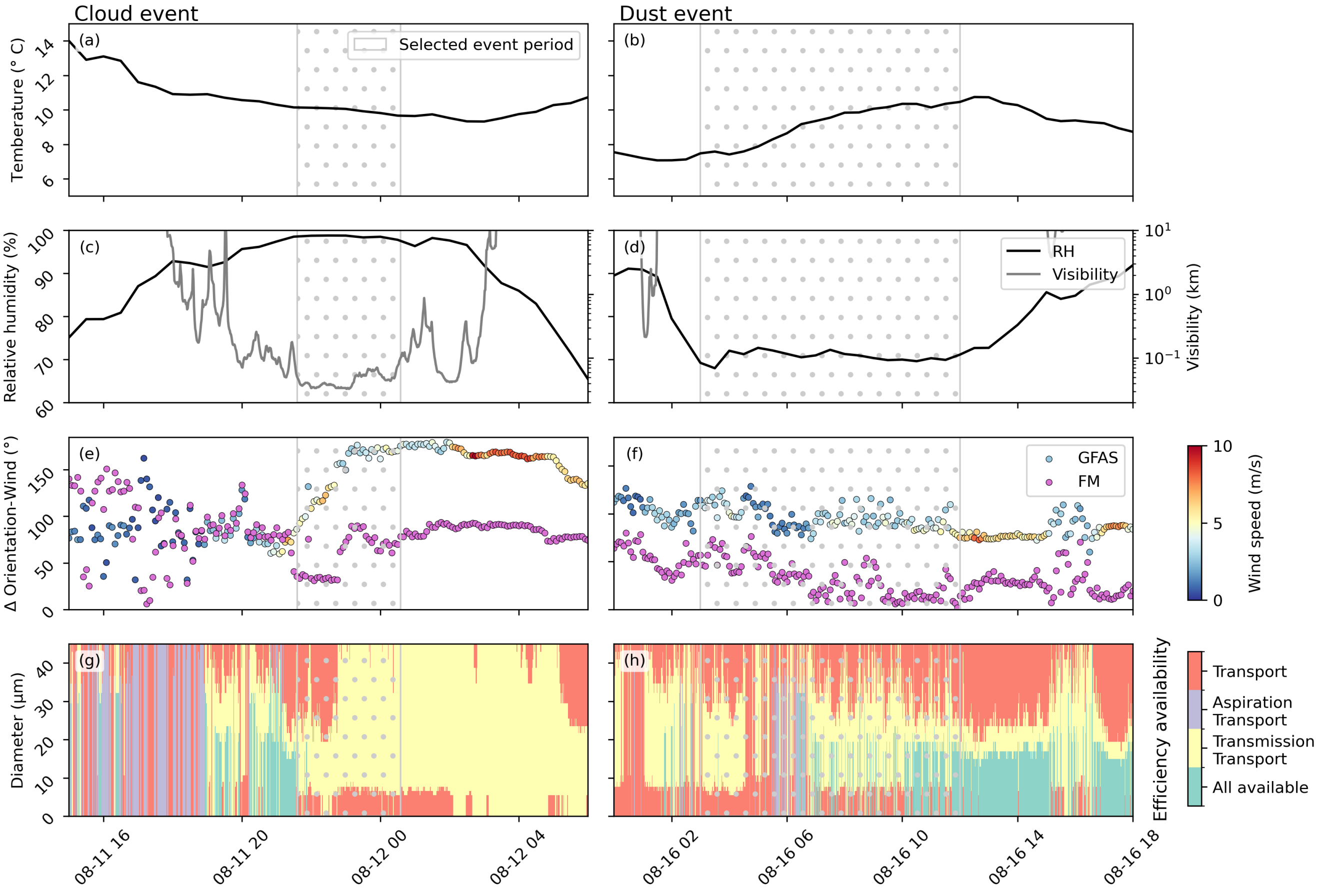

Figure S5. Auxiliary information on the cloud and dust. Temperature (a,b), relative humidity (c,d), the difference between the wind direction and inlet orientation for Ground-based Fog and Aerosol Spectrometer (GFAS) and Fog Monitor (FM) (e,f) and an indicator of where different sample efficiencies were available to apply to the GFAS (g,h). The different colors indicate which of the three sampling efficiencies could be calculated. The efficiencies are called after the description in Spiegel et al. (2012).

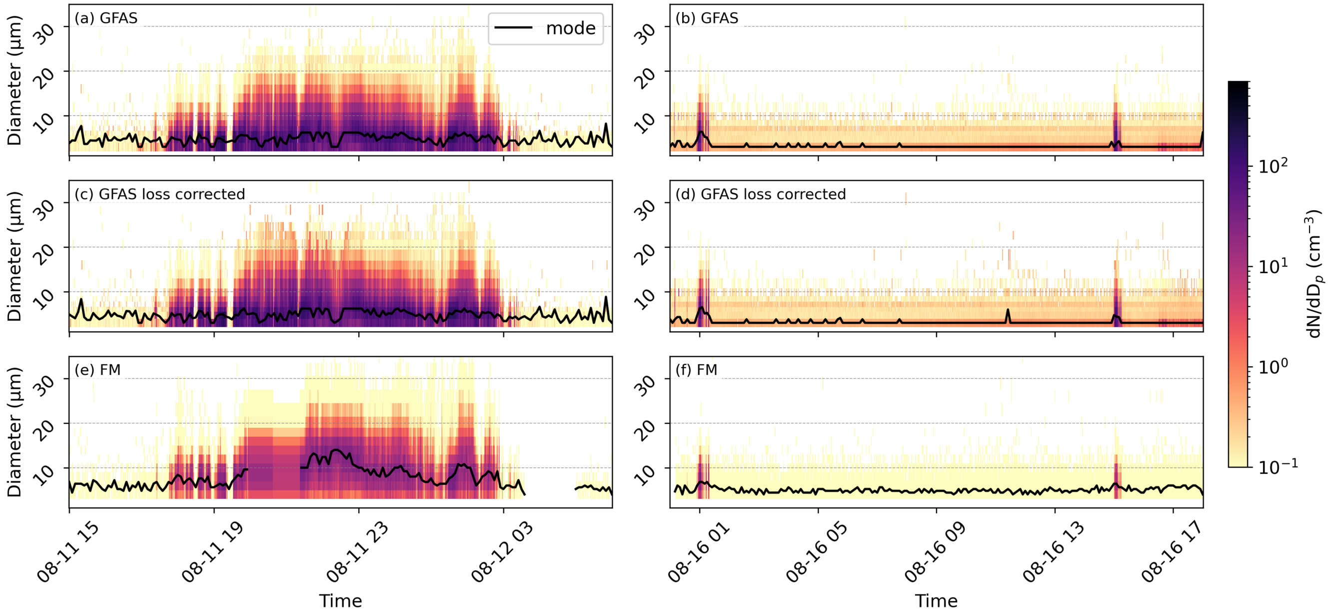

Figure S6. Size distributions for the GFAS and FM measured at SBO on June 11-12 and June 16. For the GFAS the loss un-corrected (a,b) and corrected data (c,d) are shown.

References

Spiegel, J. K., Zieger, P., Bukowiecki, N., Hammer, E., Weingartner, E., and Eugster, W.: Evaluating the capabilities and uncertainties of droplet measurements for the fog droplet spectrometer (FM-100), Atmospheric Measurement Techniques, 5, 2237–2260, https://doi.org/10.5194/amt-5-2237-2012, 2012.